








ARTICLE

Adiponectin accounts for gender differences in hepatocellular carcinoma incidence

Elisa Manieri^{1,2*} , Leticia Herrera-Melle^{1*} , Alfonso Mora¹ , Antonia Tomás-Loba¹, Luis Leiva-Vega¹, Delia I. Fernández¹, Elena Rodríguez¹, Laura Morán^{3,4} , Lourdes Hernández-Cosido⁵, Jorge L. Torres⁵, Luisa M. Seoane^{6,7}, Francisco Javier Cubero^{3,4} , Miguel Marcos⁵ , and Guadalupe Sabio¹ 

Hepatocellular carcinoma (HCC) is the sixth most common cancer type and the fourth leading cause of cancer-related death. This cancer appears with higher incidence in men and during obesity; however, the specific mechanisms underlying this correlation are unknown. Adipose tissue, a key organ in metabolic syndrome, shows evident gender disparities in the production of adipokines. Levels of the important adipokine adiponectin decrease in men during puberty, as well as in the obese state. Here, we show that this decrease in adiponectin levels is responsible for the increased liver cancer risk in males. We found that testosterone activates the protein JNK in mouse and human adipocytes. JNK-mediated inhibition of adiponectin secretion increases liver cancer cell proliferation, since adiponectin protects against liver cancer development through the activation of AMP-activated protein kinase (AMPK) and p38 α . This study provides insight into adipose tissue to liver crosstalk and its gender relation during cancer development, having the potential to guide strategies for new cancer therapeutics.

Introduction

Hepatocellular carcinoma (HCC) is the fourth leading cause of cancer-related death (Bray et al., 2018), and its incidence is rising worldwide due to the increased prevalence of obesity (Parkin et al., 2005). Therapeutic options for HCC are limited, and survival after diagnosis is poor. Better preventive, diagnostic, and therapeutic tools are therefore urgently needed, particularly in view of the important contribution of obesity to HCC incidence worldwide (Bakiri and Wagner, 2013). In addition, epidemiological studies have shown a higher incidence of HCC in men than in women (Bosch et al., 2004), a dimorphism also observed in mouse models (Ghebranious and Sell, 1998; Naugler et al., 2007). Adipose tissue is one of the most important players in the adaptation to obesity, through the regulation of fuel metabolism storage, the release of nutrients and, indirectly, the production of circulating adipokines (Havel, 2002). However, this tissue responds differently in males and females, due to the different genetic make-up and differences in the inputs that act on it (Fuente-Martín et al., 2013). The adipokine adiponectin improves hepatic insulin sensitivity and fuel oxidation

(Whitehead et al., 2006) and is considered to play a protective role in cancer (Dalamaga et al., 2012). However, its role in HCC is controversial and requires further investigation (Cheung and Cheng, 2016). Circulating adiponectin levels have been reported to show a gender disparity, being higher in females than in males (Yannakoulia et al., 2003). It has been suggested that testosterone might play a role in adiponectin levels, whereas estrogens do not seem to mediate this effect (Nishizawa et al., 2002). Here, we demonstrate that lower adiponectin levels in males account for their higher prevalence of liver cancer. We show that p38 α and AMP-activated protein kinase (AMPK) activation in hepatocytes by adiponectin results in a protective effect against tumor growth. Furthermore, we found that testosterone activates JNK in human and mouse adipocytes, and genetic deletion of JNK1 in mouse adipose tissue results in higher adiponectin levels and protection against HCC. Our results unravel a clear crosstalk between sex hormones and adipocytes signaling and physiology, clarifying the mechanism underlying gender disparity in liver cancer development.

¹Centro Nacional de Investigaciones Cardiovasculares (CNIC), Madrid, Spain; ²Centro Nacional de Biotecnología, Madrid, Spain; ³Department of Immunology, Ophthalmology and Otorhinolaryngology, Complutense University School of Medicine, Madrid, Spain; ⁴12 de Octubre Health Research Institute, Madrid, Spain; ⁵University of Salamanca, University Hospital of Salamanca–Instituto de Investigación Biomédica de Salamanca, Salamanca, Spain; ⁶Fisiopatología Endocrina, Instituto de Investigación Sanitaria de Santiago, Hospital Clínico Universitario de Santiago de Compostela Servicio Gallego de Salud, Santiago de Compostela, Spain; ⁷Centro de Investigación Biomédica en Red (CIBER), Fisiopatología Obesidad y Nutrición, Instituto Salud Carlos III, Spain.

*E. Manieri and L. Herrera-Melle contributed equally to this paper; Correspondence to Guadalupe Sabio: gsabio@cnic.es; E. Manieri's present address is Dana-Farber Cancer Institute, Boston, MA.

© 2019 Manieri et al. This article is distributed under the terms of an Attribution–Noncommercial–Share Alike–No Mirror Sites license for the first six months after the publication date (see <http://www.rupress.org/terms/>). After six months it is available under a Creative Commons License (Attribution–Noncommercial–Share Alike 4.0 International license, as described at <https://creativecommons.org/licenses/by-nc-sa/4.0/>).

Results

Increased levels of adiponectin in females protect against liver cancer

Using a cohort of healthy subjects, we found that adiponectin levels are higher in women compared with men (Fig. 1 a). Quantification of circulating adiponectin in 11–12-wk-old C57BL/6J mice confirmed previous findings, detecting more than twice the level in females than in males (Fig. S1 a). This correlated with the stronger growth of subcutaneously implanted mouse HCC-derived tumor cells in males than in females (Fig. 1 b). In addition, gender differences were HCC-specific, given that growth of subcutaneously injected colon adenocarcinoma-derived tumor cells (Fig. S1 b) or melanoma-derived tumor cells (Fig. S1 c) was not different between males and females. To further study how gender could affect adiponectin levels and, as a consequence, tumor growth, we assessed the effect of castration on blood adiponectin levels. Castrated males presented similar adiponectin levels to those found in females (Fig. 1 c). In line with the important role of adiponectin in gender disparity, castrated males developed smaller tumors in allograft experiments (Fig. 1 d). To determine whether the gender differences in adiponectin production influences tumor growth, we performed allograft experiments in male and female adiponectin KO (*Adipoq*^{-/-}) and WT mice. In WT mice, we observed larger tumors in males than in females, whereas *Adipoq*^{-/-} mice showed no gender differences (Fig. 1 e). Adiponectin cellular function is mainly mediated by two transmembrane receptors, known as adiponectin receptors 1 and 2 (AdipoR1/2; Wang and Scherer, 2016). Increased expression of both receptors were found in HCC-derived cells in comparison with colon adenocarcinoma and melanoma cells (Fig. S2 a). In the liver, hepatocytes are the main source of AdipoR2, while AdipoR1 is expressed in hepatocytes, Kupffer cells (KCs), and endothelial cells (ECs; Fig. S2 b). In addition, hepatocytes increase the expression of both receptors when they become tumoral (Fig. S2 c).

To evaluate the importance of these receptors in the protection observed in females, we used shRNAs against them in Hep53.4 cells and performed an allograft experiment in females (Fig. S2 d). Only depletion of AdipoR2 was sufficient to block the protection found in females, as no differences in tumor growth were found between males and females injected with Hep53.4 AdipoR2-shRNA-treated cells (Fig. S2 e).

The contribution of adiponectin to HCC development was evaluated by the diethylnitrosamine (DEN)-induced hepatocarcinogenesis model (Heindryckx et al., 2009). At postnatal day (P) 1, male mice were injected with a serotype 8 adeno-associated virus overexpressing adiponectin under the control of the adipocyte aP2 promoter (AAV-aP2-Adipoq) or carrying an empty control vector (AAV-aP2-CTRL). After 14 d, these mice received i.p. DEN injections to induce HCC. Adiponectin overexpression was confirmed by measurement of adiponectin plasma levels 3 wk after virus injection (Fig. S3 a), as well as 8.5 mo after virus injection (Fig. S3 b). Quantification of tumors 8 mo after DEN treatment revealed a significant reduction in the number of tumors in adiponectin-overexpressing

males (Fig. 1, f–i), indicating that adiponectin reduces tumor progression and may be a potential treatment for HCC. To further evaluate the protective effects of adiponectin in females, we used the DEN-induced HCC model in WT and *Adipoq*^{-/-} mice. Results showed that lack of adiponectin slightly increases the number of tumors 8 mo after DEN treatment (Fig. S3, c and d), corroborating that high levels of adiponectin in females contribute to the protection against HCC.

Lack of JNK1 in the adipose tissue protects against HCC progression

It is known that adipose tissue JNK controls the production of important adipokines that regulate liver metabolism (Sabio et al., 2008; Manieri and Sabio, 2015). We therefore tested whether sex-dependent differences in JNK activation in adipose tissue could account for the higher adiponectin levels in females. Western blot analysis revealed a higher activation of adipose tissue JNK in males than in females, both in mouse and rat models, which correlated with lower adiponectin levels (Fig. 2 a; Fig. S1 a; and Fig. S4, a and b), suggesting a general effect conserved among species. In line with these results, testosterone activated JNK in both mouse and human adipocytes (Fig. 2 b and Fig. S4 c). To check whether testosterone was also able to regulate JNK phosphorylation in vivo, we castrated WT male mice and performed testosterone replacement. Adipose tissue JNK activation was significantly reduced in castrated males, whereas testosterone injection was enough to increase its activation to noncastrated mice levels within 2 wk (Fig. 2 c). Importantly, the observed changes in JNK phosphorylation were in concordance with adiponectin levels, which decreased to the levels of noncastrated mice when testosterone replacement was performed (Fig. 2 d). We next examined serum concentrations of adiponectin in males with adipose tissue-specific deletion of JNK1 (F^{KO}) or control mice (F^{WT}; Fig. S5 a). Blood adiponectin levels were significantly higher in F^{KO} males than in F^{WT} males (Fig. S5 b), whereas no between-genotype differences were found in the levels of TNF α , IL-1 β , or IL-6 (Fig. S5 c). We next performed allograft tumor formation assays in F^{WT} and F^{KO} males to investigate the role of adipose tissue JNK1 in tumor growth. Consistent with the higher adiponectin levels found in F^{KO} males (Fig. S5 b), tumor growth in these mice was slower than in F^{WT} controls, and postmortem inspection revealed smaller tumors (Fig. 3 a). To further evaluate these results, F^{KO} and F^{WT} males were injected with DEN, and tumors were examined 8 mo later. We found that HCC was strongly suppressed in F^{KO} mice (Fig. 3 b). Moreover, F^{KO} mice had significantly fewer tumors than F^{WT} mice (Fig. 3 c), and tumor size and maximum tumor size were significantly lower in F^{KO} mice (Fig. 3, d and e).

Higher levels of adiponectin in F^{KO} mice are essential for their protection against HCC

To evaluate the potential role of adiponectin in the protection against HCC in F^{KO} males, we crossed WT and JNK1-deficient mice with mice deficient in adiponectin (*Adipoq*^{-/-}),

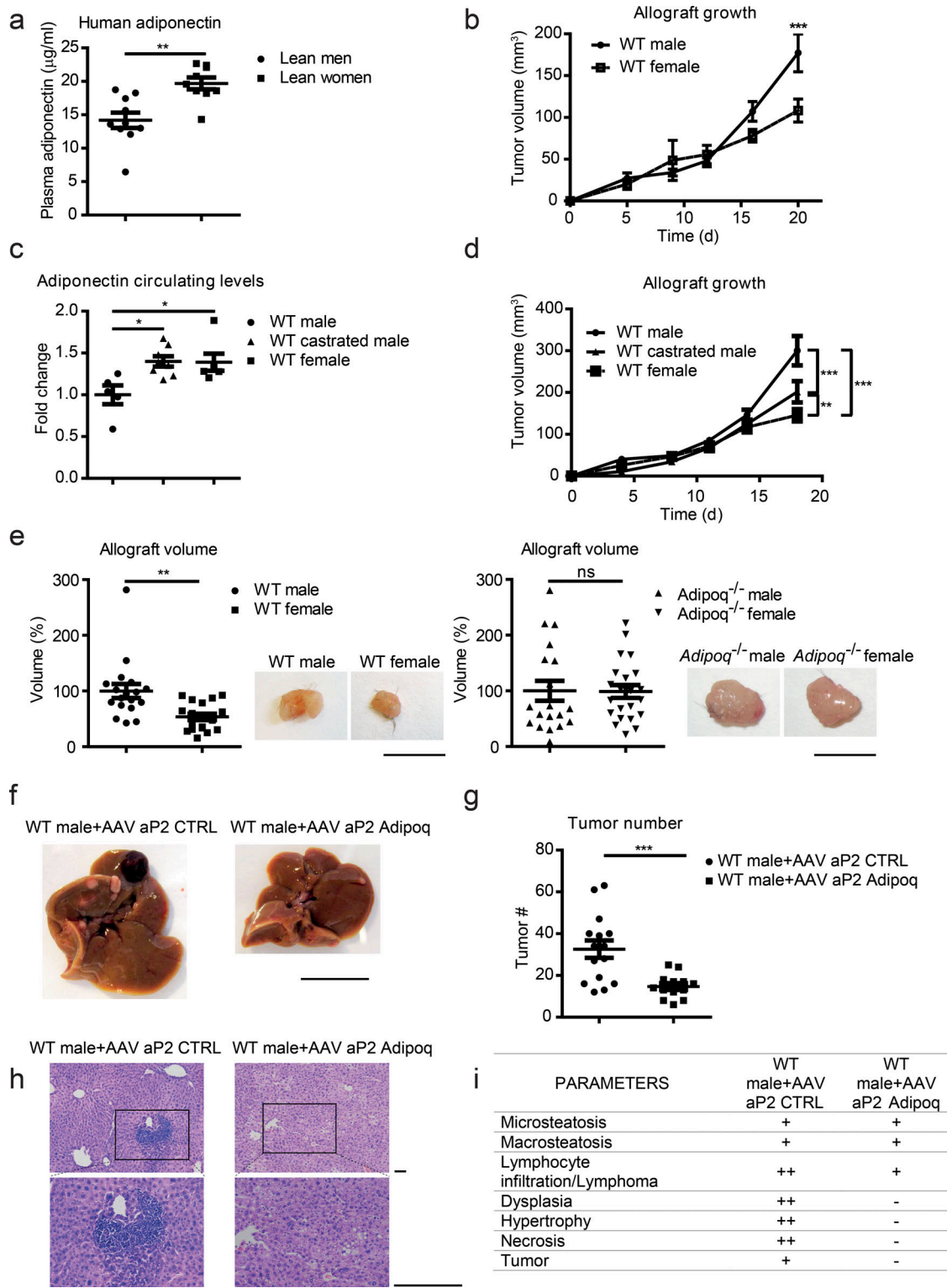


Figure 1. Adiponectin gender disparity and the effect on HCC development. (a) Quantification of circulating adiponectin levels in plasma samples from lean men and women. Data are shown as means \pm SEM; **, $P < 0.01$; Student's *t* test; men $n = 10$; women $n = 9$. (b) Tumor volume in WT male and female mice monitored over 3 wk after subcutaneous injection with 5×10^4 Hep53.4 cells in each flank. Data are shown as means \pm SEM; ***, $P < 0.001$; two-way ANOVA coupled with Bonferroni's multiple comparisons test; $n = 18$ –19 tumors (10 mice per condition). (c) Quantification of circulating adiponectin levels in 11–12-wk-old female, male, and castrated male mice. Data are normalized to WT male and are shown as means \pm SEM; *, $P < 0.05$; one-way ANOVA coupled with Bonferroni's multiple comparisons test; WT male $n = 5$; WT castrated male $n = 8$; WT female $n = 6$. (d) Tumor volume in male, female, and castrated male mice monitored over 3 wk after subcutaneous injection with 5×10^4 Hep53.4 cells in each flank. Data are shown as means \pm SEM; **, $P < 0.01$; ***, $P < 0.001$; two-way ANOVA coupled with Bonferroni's multiple comparisons test; $n = 20$ tumors (10 mice per condition), except WT castrated males $n = 18$ (9 mice). (e) Representative allografts and tumor volume quantification in WT and *Adipoq*^{-/-} male and female mice at sacrifice, 3 wk after subcutaneous

injection with 5×10^4 Hep53.4 cells in each flank. Data are shown as means \pm SEM; **, $P < 0.01$; nonsignificant differences in *Adipoq*^{-/-} mice were found (ns); Student's *t* test; WT $n = 18$ –19 tumors (10 mice per gender); *Adipoq*^{-/-} $n = 19$ –22 tumors (10 male and 11 female mice). Bar, 1 cm. **(f–i)** WT mice were injected at P1 with adeno-associated virus carrying a control sequence (AAV aP2 CTRL) or the adiponectin gene under control of the aP2 promoter (AAV aP2 Adipoq). **(f)** HCC development 8 mo after i.p. injection with DEN (50 mg/kg) on P14. Bar, 1 cm. **(g)** Tumor number was determined at sacrifice. Data are shown as means \pm SEM; ***, $P < 0.001$; Student's *t* test; WT male+AAV aP2 CTRL $n = 15$; WT male+AAV aP2 Adipoq $n = 13$. AAV, adeno-associated virus; CTRL, control. **(h)** Representative photos of H&E-stained liver sections obtained from these DEN-injected mice at sacrifice (upper panels: 10 \times ; lower panels: 20 \times ; bars, 100 μ m). **(i)** Histopathological evaluation was performed in livers from these mice upon sacrifice. No injury (-) or different grades of injury (mild [+], moderate [++], or marked [+++]) were noted in at least seven view fields per slide. $n = 10$ per condition.

and repeated the allograft assays. Tumor growth was identical in F^{WT}*Adipoq*^{-/-} and F^{KO}*Adipoq*^{-/-} males (Fig. 4 a), consistent with a central role for adiponectin in the F^{KO} phenotype, and suggesting that the elevated adiponectin levels in F^{KO} males were responsible for their reduced tumor growth. To corroborate this hypothesis, we analyzed DEN-induced liver cancer in F^{WT}*Adipoq*^{-/-} and F^{KO}*Adipoq*^{-/-} males. Tumor number, size, and maximum size after 8 mo did not differ significantly between the two groups of mice, suggesting an important role for adiponectin in the protection of F^{KO} males against DEN-induced HCC (Fig. 4, b–e).

AMPK α and p38 α activation by adiponectin reduces tumor progression

Adiponectin transduces its signal in the liver through the activation of two pathways: p38 MAPK (Mao et al., 2006a,b) and AMPK (Yamauchi et al., 2002; Polyzos et al., 2010). p38 α suppresses liver cancer development by reducing cell proliferation, and consequently, mice with hepatic deletion of p38 α show enhanced hepatocyte proliferation and tumor development (Hui et al., 2007). AMPK also suppresses cancer, and treatment with the AMPK activator metformin reduces cancer incidence (Chen et al., 2013) and may improve survival among liver cancer patients (Ma et al., 2016). Consequently, AMPK is emerging as an important metabolic tumor suppressor and a promising target for cancer prevention and therapy (Luo et al., 2010). We evaluated the activation of AMPK and p38 α in allografts from male and female mice. Immunoblot analysis detected higher levels of AMPK and p38 α activation (phosphorylation) in females (Fig. 5 a), correlating with the higher adiponectin levels in female mice (Fig. S1 a). This gender difference in p38 α or AMPK activation was not observed in *Adipoq*^{-/-} mice (Fig. 5 b), suggesting that higher activation of these kinases in females is the result of the higher levels of circulating adiponectin. To evaluate whether p38 α and AMPK activation is implicated in the protection against liver cancer in females, we implanted Hep53.4 cells subcutaneously into male mice and activated each pathway by two different strategies. In the first strategy, animals were treated with metformin to activate AMPK. In the second one, allografts were injected with a retrovirus containing active p38 α or a control construct on days 9 and 22 after transplantation. As expected, metformin treatment significantly reduced tumor volume (Fig. 5 c), indicating that AMPK activation confers protection against HCC. Similarly, tumors infected with active p38 α

were significantly smaller (Fig. 5 d), suggesting that the adiponectin-mediated protection against HCC is also mediated by p38 α activation.

We next investigated the extent of p38 α and AMPK phosphorylation in livers of F^{KO} mice. Consistent with the high levels of adiponectin in F^{KO} males, liver activation of p38 α and AMPK was significantly higher in DEN-treated F^{KO} male mice than in their F^{WT} counterparts (Fig. S5, d and e). To evaluate whether AMPK activation is necessary for adiponectin-mediated protection in F^{KO} mice, we treated Hep53.4 cells with shRNA against AMPK or a scrambled control sequence. As expected, AMPK knockdown in Hep53.4 cells resulted in larger tumors after implantation in F^{WT} animals. More importantly, F^{KO} males were no longer protected against tumor growth, indicating that AMPK activation in hepatocytes is necessary for the protection observed in F^{KO} mice (Fig. 5 e).

Discussion

Liver cancer is the fourth most common cause of death from cancer worldwide (Marquardt et al., 2015). The incidence and mortality rates of liver cancer have increased rapidly, coinciding with the rising prevalence of obesity (Larsson and Wolk, 2007). Accumulating epidemiological evidence indicates that excess of body weight may be a risk factor for liver cancer; however, the link between both phenomena remains elusive.

Adipose tissue is recognized as an active endocrine organ that mediates a variety of physiological functions via secretion of adipokines. Here, we found that gender differences in adipocytes are important players in HCC progression and can contribute to the increased incidence of HCC observed in males. Our study demonstrates that adiponectin plays an important role in protecting female mice against HCC. In men, adiponectin levels decrease with puberty, whereas its levels are maintained in women (Böttner et al., 2004). A similar gender disparity occurs in mice (Combs et al., 2003). We found that the gender bias in tumor growth is strongly dependent on adiponectin, and that adiponectin KO mice showed no gender differences in tumor progression. We also demonstrate that activation of JNK in adipose tissue correlates with reduced levels of adiponectin in males, and that males with JNK1 deficiency in adipose tissue have increased adiponectin secretion, protecting against HCC. Moreover, castration reduces JNK phosphorylation in the adipose tissue while testosterone replacement increases it, together with a reduction in adiponectin to the levels before castration.

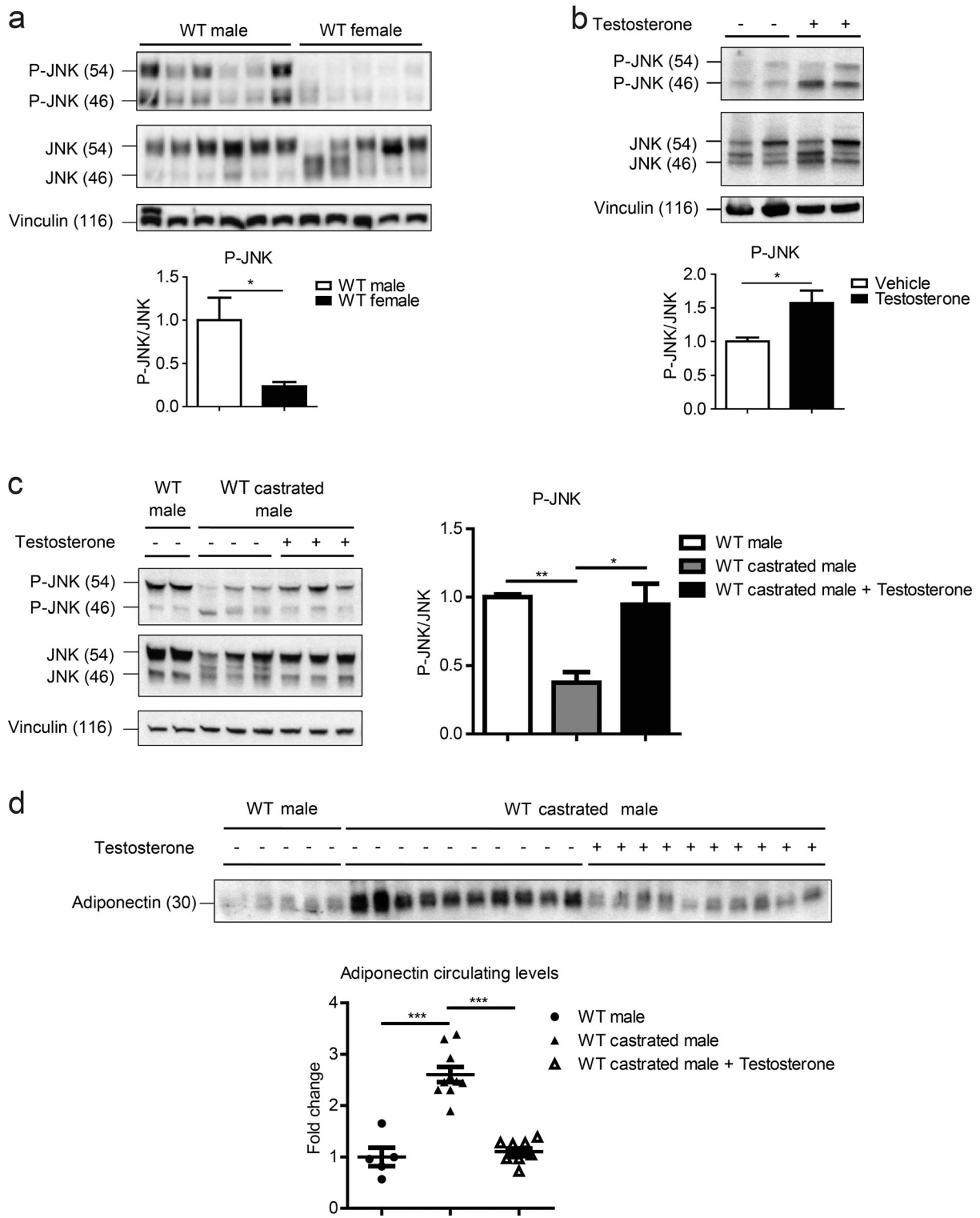


Figure 2. **Effect of testosterone on the control of adiponectin levels through adipose tissue JNK.** (a) Immunoblot analysis and quantification of phospho (P)-JNK and JNK in adipose tissue from WT male and female rats. Vinculin protein expression was monitored as a loading control. Data are shown as means \pm SEM; *, $P < 0.05$; Student's *t* test; WT male $n = 6$; WT female $n = 5$. (b) Immunoblot analysis and quantification of phospho-JNK and JNK in mouse differentiated adipocytes after treatment with testosterone (300 nM for 120 min). Vinculin protein expression was monitored as a loading control. Data are shown as means \pm SEM; *, $P < 0.05$; Student's *t* test; $n = 3$. (c and d) 4-wk-old WT males were castrated or sham-operated and they were subcutaneously injected with testosterone propionate (5 μ g/g body weight) or vehicle alone every other day for 3 wk. (c) Immunoblot analysis and quantification of phospho-JNK and JNK in adipose tissue from these WT male mice, treated with testosterone propionate (50 μ g/g body weight) or vehicle alone, 30 min before sacrifice. Vinculin protein expression was monitored as a loading control. Data are normalized to WT male and are shown as means \pm SEM; *, $P < 0.05$; **, $P < 0.01$; one-way ANOVA coupled with Bonferroni's multiple comparisons test; $n = 3$, except WT sham males $n = 4$. (d) Immunoblot analysis and quantification of circulating adiponectin levels 2 wk after the first testosterone injection. Data are normalized to WT male and are shown as means \pm SEM; ***, $P < 0.001$; one-way ANOVA coupled with Bonferroni's multiple comparisons test; $n = 10$, except WT sham males $n = 5$.

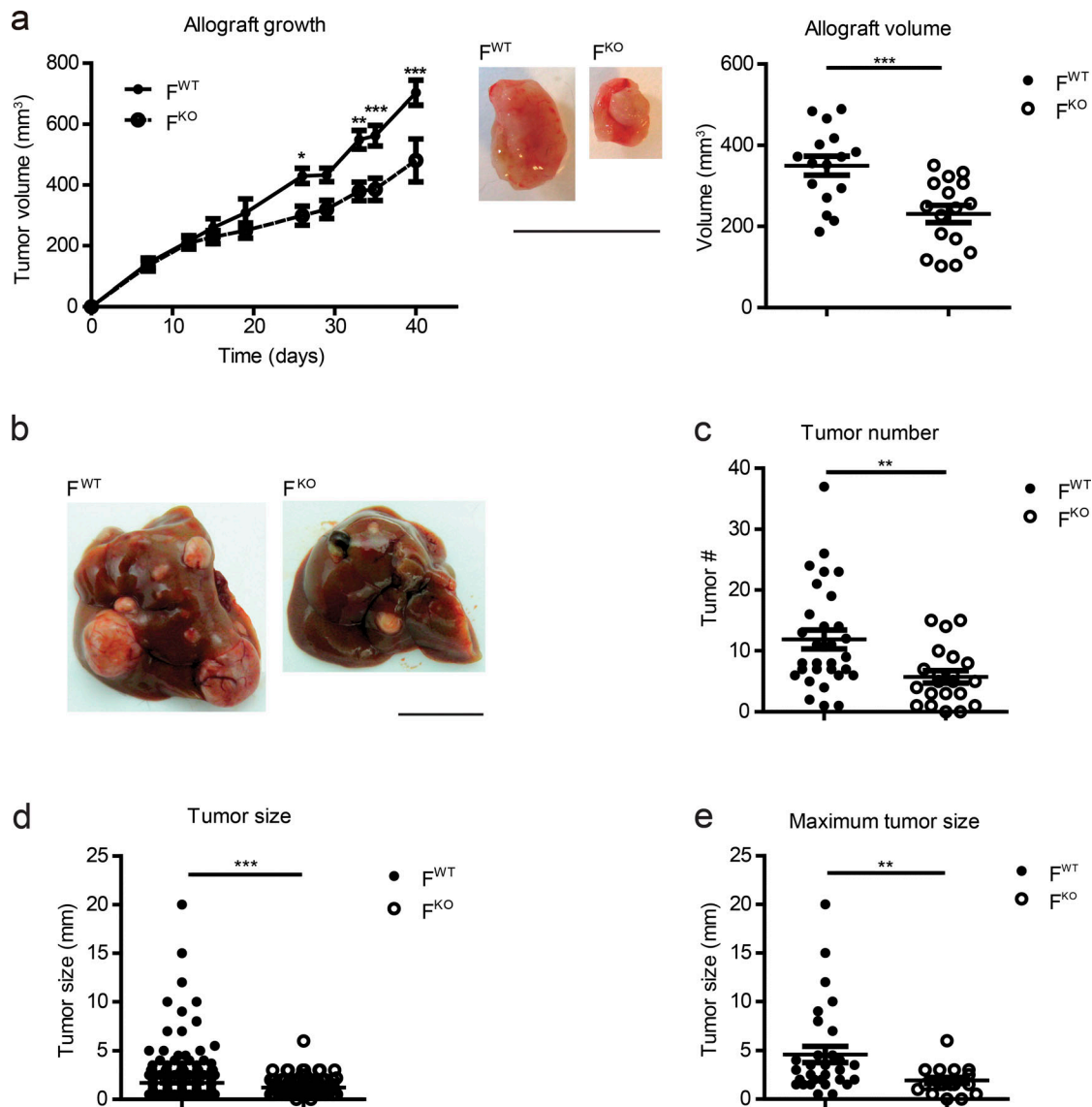


Figure 3. Effect of adipose tissue JNK1 deficiency on HCC progression. (a) Representative allografts and tumor volume quantification in F^{WT} and F^{KO} male mice during the experiment and at sacrifice 5 wk after subcutaneous injection with 5×10^4 Hep53.4 cells in each flank. Data are shown as means \pm SEM; *, $P < 0.05$; **, $P < 0.01$; ***, $P < 0.001$; two-way ANOVA coupled with Bonferroni's multiple comparisons test (allograft growth); Student's *t* test (allograft volume); $n = 16$ –18 tumors (8–9 mice per genotype). Bar, 1 cm. (b–e) HCC progression analyzed in control (F^{WT}) and adipose tissue JNK1-deficient (F^{KO}) mice 8 mo after i.p. injection with DEN (50 mg/kg body weight) on P14. (b) Representative images of liver tumors in F^{WT} and F^{KO} mice. Bar, 1 cm. (c–e) Tumor number, tumor size, and maximum tumor size. Data are shown as means \pm SEM; **, $P < 0.01$; ***, $P < 0.001$; Student's *t* test (tumor number); Student's *t* test with Welch's correction (tumor size and maximum tumor size); F^{WT} $n = 30$; F^{KO} $n = 20$ –21.

These results indicate that activation of JNK in adipose tissue inhibits adiponectin secretion, promoting tumor growth in males. Epidemiological studies suggest the association between low adiponectin levels and liver tumorigenesis (Kotani et al., 2009). In line with this, adiponectin has an anti-oncogenic potential in HCC cell lines (Sharma et al., 2010). However, opposite results were reported for HCC associated with hepatitis C (Arano et al., 2011). These discrepancies may be attributable to the different HCC etiologies examined in those studies (Dalamaga et al., 2012). Here, using mouse models, we demonstrated that adiponectin protects against HCC by activating p38 α and AMPK. Our results suggest that adiponectin and metformin could be of use in the treatment of HCC.

Materials and methods

Study population and sample collection

For the analysis of human levels of blood adiponectin, individuals were recruited among patients who underwent laparoscopic cholecystectomy for gallstone disease.

Blood was extracted using straight needles (21G butterfly) and Vacuette Z Serum Sep Clot Activator tubes. After 30 min, these tubes were centrifuged at 1,500 rpm for 10 min at room temperature to separate serum, which was divided into aliquots and stored at -80°C until further analysis. The study was approved by the Ethics Committee of the University Hospital of Salamanca, and all subjects provided written informed consent to participate. Fasting blood samples were

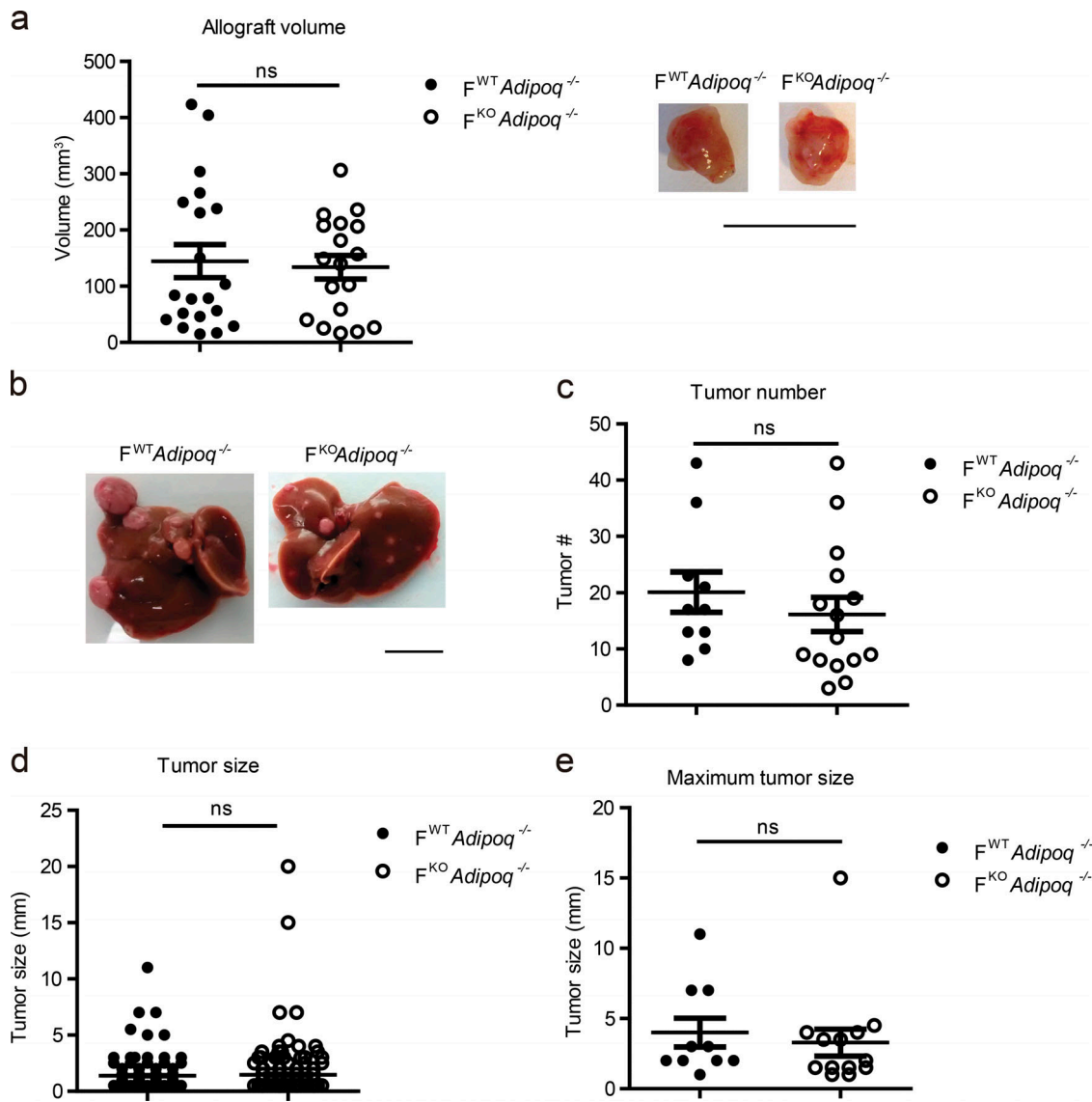


Figure 4. **High levels of adiponectin in F^{KO} mice are responsible for the protection against HCC.** (a) Tumor volume quantification and representative allografts in male F^{WT} adiponectin KO mice ($F^{WT}Adipoq^{-/-}$) and male F^{KO} adiponectin KO mice ($F^{KO}Adipoq^{-/-}$) at sacrifice 5 wk after subcutaneous injection of 5×10^4 Hep53.4 cells in each flank. Data are shown as means \pm SEM; nonsignificant differences were found (ns); Student's *t* test; $F^{WT}Adipoq^{-/-}$ *n* = 20 tumors (10 mice); $F^{KO}Adipoq^{-/-}$ *n* = 18 tumors (9 mice). Bar, 1 cm. (b–e) HCC progression analyzed in $F^{WT}Adipoq^{-/-}$ and $F^{KO}Adipoq^{-/-}$ mice 8 mo after i.p. injection with DEN (50 mg/kg body weight) on P14. (b) Representative images of liver tumors in $F^{WT}Adipoq^{-/-}$ and $F^{KO}Adipoq^{-/-}$ mice. Bar, 1 cm. (c–e) Tumor number, tumor size, and maximum tumor size. Data are shown as means \pm SEM; nonsignificant differences were found (ns); Student's *t* test; $F^{WT}Adipoq^{-/-}$ *n* = 10; $F^{KO}Adipoq^{-/-}$ *n* = 15.

collected for adiponectin, glucose, and lipid analysis. Patients were excluded if they had a history of alcohol use disorders or excessive alcohol consumption (>30 g/d in men and >20 g/d in women), chronic hepatitis C or B, or body mass index \geq 35 (Table S1).

Animals

Adiponectin KO mice (B6;129-Adipoq^{tm1Chan/J}) and FabP4 cre mice (B6.Cg-Tg(Fabp4-cre)1Rev/J) were purchased from the Jackson Laboratory and backcrossed to the C57BL/6 background for 10 generations. Mice with specific deletion of JNK1 in adipocytes (F^{KO}) were as described (Sabio et al., 2008), and F^{WT} littermates were used as controls. Mice were housed randomly in a

pathogen-free animal facility and maintained on a 12-h light/dark cycle at constant temperature and humidity. Genotypes were identified by PCR analysis of genomic DNA isolated from mouse tails. For tumor studies, mice at P14 received one i.p. injection of DEN (Sigma-Aldrich) at 50 mg/kg body weight dissolved in saline. After 8 mo, tumors were extracted and measured with a caliper. In all cases, mice were euthanized after overnight starvation. For testosterone deprivation studies, castration or sham operations were performed in mice at 4–5 wk of age. 23 d after castration, testosterone propionate (Desma) diluted in corn oil (5 μ g/g body weight) or vehicle alone was subcutaneously injected in castrated or sham-operated mice, every other day for 3 wk. Blood samples were collected 2 wk

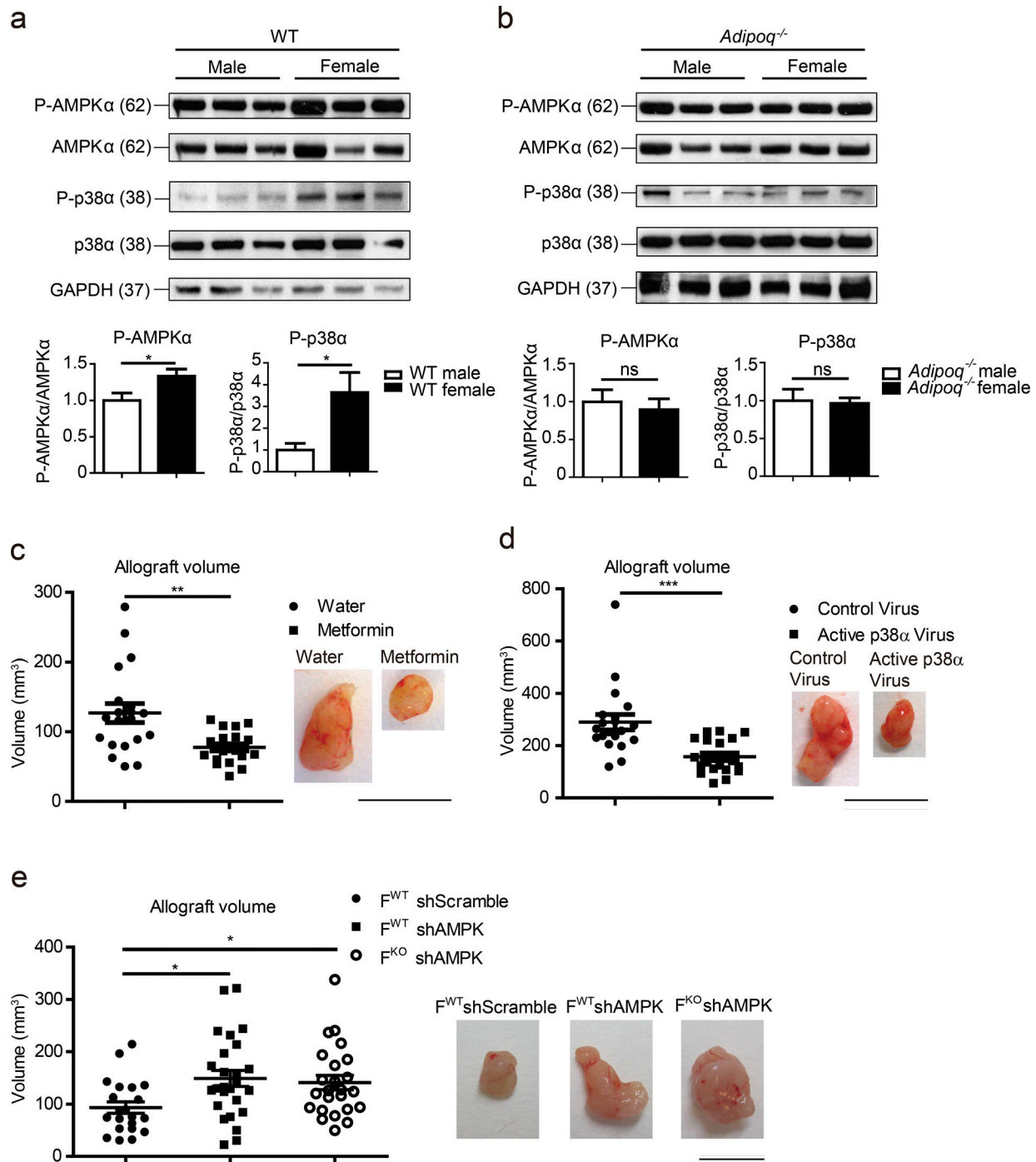


Figure 5. AMPK α and p38 α activation protects against tumor growth. (a) Immunoblot analysis and quantification of phospho-AMPK α , AMPK α , phospho-p38 α , and p38 α in tumor allografts obtained from WT male and female mice 21 d after implantation. GAPDH protein expression was monitored as a loading control. Data are shown as means \pm SEM; *, $P < 0.05$; Student's t test; WT male $n = 10$; WT female $n = 6-9$. (b) Immunoblot analysis and quantification of phospho-AMPK α , AMPK α , phospho-p38 α , and p38 α in tumor allografts obtained from *Adipoq*^{-/-} male and female mice 21 d after implantation. GAPDH protein expression was monitored as a loading control. Data are shown as means \pm SEM; nonsignificant differences were found (ns); Student's t test; *Adipoq*^{-/-} male $n = 10$; *Adipoq*^{-/-} female $n = 11$. (c) Representative allografts and tumor volume quantification in WT male at sacrifice 5 wk after subcutaneous injection with 5×10^4 Hep53.4 cells in each flank and treatment with 300 mg/d \cdot kg body weight of metformin (supplied in the drinking water). Data are shown as means \pm SEM; **, $P < 0.01$; Student's t test with Welch's correction; $n = 20$ tumors (10 mice per genotype). Bar, 1 cm. (d) Representative allografts and tumor volume quantification in WT male overexpressing p38 α in hepatic tumors. Mice received subcutaneous injections in each flank with 5×10^4 Hep53.4 cells followed by intratumor injections on days 9 and 22 with retrovirus expressing active p38 α or control virus. Male mice were sacrificed 5 wk after Hep53.4 cell injection. Data are shown as means \pm SEM; ***, $P < 0.001$; Student's t test with Welch's correction; $n = 20$ tumors (10 mice per genotype). Bar, 1 cm. (e) Representative allografts and tumor volume quantification in WT male with hepatic tumors lacking AMPK expression. Mice received subcutaneous injections in each flank with 1×10^6 Hep53.4 cells in each flank, previously transduced with shRNA targeting AMPK or a control sequence (shScramble). Mice were sacrificed 5 wk after Hep53.4 cell injection. Data are shown as means \pm SEM; *, $P < 0.05$; one-way ANOVA coupled with Dunnett's multiple comparisons test. F^{WT}shScramble $n = 21$ tumors (11 mice); F^{WT}shAMPK $n = 26$ tumors (13 mice); F^{KO}shAMPK $n = 24$ tumors (12 mice). Bar, 1 cm.

after the first injection, and testosterone propionate (50 µg/g body weight) was injected into some castrated mice 30 min before sacrifice, at the end of the experiment. For healthy and tumor hepatocytes analysis, C57BL/6J mice were injected with a single dose of DEN at day 14 postnatally, followed by administration of thioacetamide (TAA; 300 µg/liter) in the drinking water during 26 wk as described in [Salguero Palacios et al. \(2008\)](#). Control mice received a single injection of PBS at day 14 and normal drinking water. The parenchymal and the non-parenchymal compartment was isolated from vehicle (healthy) or DEN/TAA (tumor) mice. All animal experiments conformed to European Union Directive 2010/63EU and Recommendation 2007/526/EC, enforced in Spanish law under Real Decreto 1386/2018. All experiments were approved for the Centro Nacional de Investigaciones Cardiovasculares Carlos III ethics committee and Comunidad de Madrid.

Adeno-associated virus

Male mice were injected intravenously at P1 with 0.5×10^{11} viral particles of a serotype 8 adeno-associated virus overexpressing adiponectin under the control of the adipocyte-specific aP2 mini promoter (lentiviral vector tailor-designed and purchased from Vector Builder) or carrying an empty control vector.

Serum analysis

Serum cytokine concentrations were measured by multiplexed ELISA in a Luminex 200 analyzer (Millipore).

Adiponectin was detected in plasma samples by Western blot. Samples were diluted in PBS (1:10) and buffered with 2× Native Tris-Glycine Sample Buffer (Invitrogen). Diluted samples were loaded on precast native gels to preserve adiponectin multimers (NativePAGE Bis-Tris gel system; Thermo Fisher Scientific) and run with Novex Tris-Glycine Native Running Buffer (Invitrogen). In other cases, plasma samples were prepared as described but diluted in PBS, Milli-Q water, and Laemmli Sample Buffer and separated by SDS-PAGE. Membranes were blocked with 10% milk prepared in PBS without detergents (in the first case) or with PBS-Tween 0.1% (in the second case), and probed with a primary antibody to adiponectin (1:500 dilution; PA1-054; Thermo Fisher Scientific). After washing, membranes were incubated with a fluorescent secondary antibody (goat anti-rabbit 680 nm 926-32221; Odyssey) or a horseradish peroxidase-conjugated secondary antibody (GE Healthcare), and proteins were visualized and quantified using the Odyssey LI-COR imaging system (LI-COR) or an enhanced chemiluminescent substrate (Clarity Western ECL substrate; Bio-Rad), respectively. We assured the specificity of the antibody using serum from *Adiponectin* KO mice. Results were normalized to the control group (male mice or F^{WT} or control mice, as indicated in the figure legends).

Biochemical analysis

Total proteins from different organs or from adipocytes were extracted in lysis buffer (50 mM Tris-HCl, pH 7.5, 1 mM EGTA, 1 mM EDTA, pH 8.0, 50 mM NaF, 1 mM sodium glycerophosphate, 5 mM pyrophosphate, 0.27 M sucrose, 1% Triton X-100, 0.1 mM PMSF, 0.1% 2-mercaptoethanol, 1 mM sodium

orthovanadate, 1 µg/ml leupeptin, and 1 µg/ml aprotinin) and centrifuged at $8,600 \times g$ for 20 min at 4°C. Extracts were separated by SDS-PAGE and transferred to 0.2-µm-pore-size nitrocellulose membranes (Bio-Rad). Blots were probed with primary antibodies to phospho-JNK (Thr183/Tyr185; 4668), total JNK (9252), phospho-AMPKα (Thr172; 2531), total AMPKα (2603), and phospho-p38 (Thr180/Tyr182; 9211; all from Cell Signaling Technology), p38 from Santa Cruz Biotechnology (sc-535), and GAPDH (sc-25778) and vinculin (V4505; Sigma-Aldrich). All antibodies were used at 1:1,000. After washes, membranes were incubated with an appropriate horseradish peroxidase-conjugated secondary antibody (GE Healthcare), and signals were detected using an enhanced chemiluminescent substrate (Clarity Western ECL substrate; Bio-Rad). Protein levels were analyzed by optical density measured with ImageJ (National Institutes of Health). Results were normalized to the not phosphorylated form.

Allografts

The Hep53.4 cell line was purchased from CLS-Cell Lines Service and tested against *Mycoplasma* (MycoAlert Detection Kit; Lonza). Cells were cultured in DMEM supplemented with 10% FBS, L-glutamine, and antibiotics. The MC-38 and B16-F10 cell lines originally were tested against *Mycoplasma*. MC-38 cells were cultured in DMEM supplemented with 10% FBS, non-essential amino acids, sodium pyruvate, Hepes, L-glutamine, and antibiotics, whereas B16-10's culture medium only contained DMEM supplemented with 10% FBS, sodium pyruvate, and antibiotics. For allograft assays, Hep53.4 cells (5×10^4 cells for usual experiments, or 1×10^6 for short hairpin RNA experiments) were mixed 1:1 with Matrigel Matrix (Corning) and subcutaneously injected into each flank of anesthetized 8–12-wk-old mice. For MC-38 or B16-F10 allograft assays, 5×10^5 cells without Matrigel were subcutaneously injected into each flank. In both cases, tumor growth was monitored by measuring length and width every 3–4 d for a period of 2, 3, or 5 wk. At the end of the experiment, mice were sacrificed and tumors extracted and measured. To study AMPKα activation by metformin, mice were treated with metformin (300 mg/d · kg body weight), starting 1 wk before allograft injection. In allografts treated with active p38α, pBABE p38α D176A/F327S retrovirus was injected intratumorally on days 9 and 22.

Adipocytes cell culture

Immortalized white preadipocytes from C57BL/6 male mice were maintained in DMEM-F12 medium with 8% FBS, 200 mM L-glutamine, and 10,000 U/ml penicillin/streptomycin. These cells were differentiated to white adipocytes for 10 d with the previous medium supplemented with 5 µg/ml insulin, 25 µg/ml 3-isobutyl-1-methylxanthine, 1 µg/ml dexamethasone, and 1 µM troglitazone. The cells were starved overnight and treated with 300 nM testosterone (Sigma-Aldrich) for 2 h.

Human visceral white preadipocytes were purchased from Innoprot, and culture was set up following the manufacturer's instructions. Preadipocyte differentiation medium from Innoprot was used for the differentiation to white

adipocytes during 8 d, followed by an overnight starvation and treatment with 1,200 nM testosterone or vehicle for 30 min.

Liver cell populations isolation

To isolate the different hepatic cell types, a perfusion was performed in a C57BL/6 mouse. The liver was perfused with each solution (A, B, and C; see Table S3) separately for 5 min or 25 ml. After the final solution C, the perfusion was stopped and the liver was dissected and transferred into solution D and incubated for 20 min at 37°C. To ensure proper digestion of the liver, solution D was inverted several times during the incubation time. Next, solution D containing the digested liver was filtered through a 70- μ m cell strainer, and the filtered solution was centrifuged at 50 \times *g* for 1 min at 4°C. The pellet containing hepatocytes was kept for further analysis, and the supernatant was transferred to a new conical tube and subsequently centrifuged at 720 \times *g* for 8 min at 4°C. The supernatant was removed and the pellet was resuspended in 10 ml Gey's Balanced Salt Solution buffer (GBSS-B) solution containing 150 μ l DNase I stock solution, and the conical tube was filled up to 50 ml with GBSS-B solution. In the next step, the solution was centrifuged at 720 \times *g* for 8 min at 4°C, and the supernatant was removed. Next, the pellet was resuspended in 10 ml GBSS-B containing 150 μ l DNase I stock solution. In addition, 24 ml GBSS-B and 14 ml of the Nycodenz 1 solution were added, and the solution was carefully mixed. Further, 4 ml of the Nycodenz 2 solution was transferred into six 15-ml falcon tubes. Next, 8.3 ml of the mixed cell solution containing GBSS-B, DNase, and Nycodenz 1 was carefully laid onto the Nycodenz 2 solution, and the GBSS-B solution was used to gently overlay the cell suspension to obtain a final volume of 15 ml. Consequently, the gradient solution was centrifuged without brakes at 3,000 \times *g* for 20 min at 4°C. After the centrifugation step, hepatic stellate cells (HSCs) are found in the upper gradient phase as a white ring, and KCs are found in the lower gradient phase. Each cell type was carefully transferred to a new tube and washed with GBSS-B solution and subsequently centrifuged at 720 \times *g* for 8 min at 4°C to pellet the cells. The supernatant was removed, and the cells were checked for their purity under a microscope and subsequently frozen in liquid nitrogen and stored at -80°C for further RNA isolation. See Tables S3 and S4 to check the solutions used for the isolation of different hepatic cell types.

Histological analysis

Histopathological examination of H&E-stained livers was performed in an Eclipse CiL light microscope (Nikon), using 10–20 \times magnification with a numerical aperture of 0.25–0.40 of the optic lenses. Microphotographs were taken with a Nikon Camera DS-Fi3 and acquired using the NIS-Elements Microscope Imaging Software (Nikon). Histopathological grading of chronic liver disease was assessed based on the score system previously published (Goodman, 2007), but modified for nonalcoholic fatty liver disease and HCC. No insult (-) or different grades of injury (mild [+], moderate [++], or marked [+++]) were noted in at least seven view fields per slide.

RNA analysis

Total RNA was isolated from healthy or tumorigenic hepatocytes, other cell populations in the liver (KCs, ECs, and HSCs), as well as from different tumor cell lines (Hep53.4, MC-38, and B16-F10) using the RNeasy Mini Kit (Qiagen). Complementary DNA was synthesized with the High-Capacity Complementary DNA Reverse Transcription Kit (Applied Biosystems). Sequences of primers used for quantitative real-time PCR (qRT-PCR) are provided in Table S2. Expression levels were normalized to *Gapdh* mRNA. qRT-PCR was performed using Fast SYBR Green.

Statistical analysis

Differences between groups were examined for statistical significance using the two-tailed Student's *t* test, Student's *t* test coupled with Welch's correction in case of not equal variances, or one- or two-way ANOVA coupled to Bonferroni's or Dunnett's post-test.

Online supplemental material

Fig. S1 shows the mouse gender differences of adiponectin levels and the lack of differences in the growth of colon adenocarcinoma and melanoma cells between males and females. Fig. S2 shows the analysis of adiponectin receptors expression in different tumor cells and liver cell populations, along with the growth of HCC-derived tumor cells with reduced AdipoR1 or AdipoR2 levels. Fig. S3 shows the increased adiponectin levels observed in males infected with the adeno-associated virus overexpressing adiponectin and the maintenance of these high levels until the end of the experiment, as well as the effect of lack of adiponectin in females on tumor number. Fig. S4 shows the rat gender differences of adiponectin levels, the mouse gender differences in fat JNK activation, and its activation in human adipocytes upon testosterone stimuli. Fig. S5 shows the specific deletion of JNK1 in the adipose tissue, adiponectin and cytokine levels in F^{WT} and F^{KO} mice, and higher AMPK α and p38 α activation in F^{KO} compared with F^{WT} mice. Table S1 shows the characteristics of women and men population used in the study. Table S2 shows the sequences of the primers used for the qRT-PCRs. Tables S3 and S4 show the solutions used for the isolation of different hepatic cell types, for both hepatic perfusion and hepatic cell isolation.

Acknowledgments

We thank K. McCreath and S. Bartlett for English editing. We are grateful to Dr. R.J. Davis (University of Massachusetts Medical School, Worcester, MA) for the F^{KO} animals and critical reading of the manuscript. We thank Dr. A. Nebreda (Institute for Research in Biomedicine, Barcelona, Spain) for the active pBABE p38 α D176A/F327S plasmid. We also thank Dr. David Sancho (Centro Nacional de Investigaciones Cardiovasculares [CNIC], Madrid, Spain) for the MC-38 and B16-F10 cell lines, and Centro Nacional de Investigaciones Cardiovasculares Carlos III Animal Facility for the castration of mice.

G. Sabio is an investigator on the Ramón y Cajal Program. E. Manieri is a La Caixa Foundation fellow. L. Herrera-Melle is a fellow of the Ministerio de Educación, Cultura y Deporte (FPU15-05802). This study was funded by the following grants: G. Sabio was funded by the European Research Council (ERC 260464), European Foundation for the Study of Diabetes–Lilly, Ministerio de Ciencia, Innovación y Universidades (MICINN/SAF2016-79126-R), Comunidad de Madrid (B2017/BMD-3733), and BBVA Becas Leonardo a Investigadores y Creadores Culturales (Investigadores-BBVA-2017; IN[17]_BBM_BAS_0066); M. Marcos was funded by Instituto de Salud Carlos III and Federación Española de Enfermedades Raras (PI16/01548); and J.L. Torres was funded by Junta de Castilla y León GRS (1587/A/17). F.J. Cubero is a Ramón y Cajal Researcher (RYC-2014-15242) and a Gilead Liver Research Scholar 2018, and his work is supported by the Ministerio de Economía y Competitividad Retos (SAF2016-78711), Comunidad de Madrid (S2017/BMD-3727), The Alan Morement Memorial Fund Cholangiocarcinoma Charity (2018/117), the European Cooperation in Science and Technology Action (CA17112), and the European Foundation for Alcohol Research (EA14/18). L. Morán is a Comunidad de Madrid fellow (S2017/BMD-3727). The CNIC is supported by the Ministerio de Ciencia, Innovación y Universidades and the Pro CNIC Foundation, and is a Severo Ochoa Center of Excellence (SEV-2015-0505).

The authors declare no competing financial interests.

Author contributions: G. Sabio conceived, designed, and supervised this project. E. Manieri, L. Herrera-Melle, and A. Mora designed the project, developed the hypothesis, performed the experiments, analyzed the data, and prepared figures. A. Tomás-Loba, L. Leiva-Vega, D.I. Fernández, M.E. Rodríguez, L. Morán, L. Hernández-Cosido, J.L. Torres, L.M. Seoane, F.J. Cubero, and M. Marcos participated in the experiments. E. Manieri, L. Herrera-Melle, and G. Sabio wrote the manuscript with input from all authors.

Submitted: 9 July 2018

Revised: 11 January 2019

Accepted: 8 February 2019

References

Arano, T., H. Nakagawa, R. Tateishi, H. Ikeda, K. Uchino, K. Enooku, E. Goto, R. Masuzaki, Y. Asaoka, Y. Kondo, et al. 2011. Serum level of adiponectin and the risk of liver cancer development in chronic hepatitis C patients. *Int. J. Cancer*. 129:2226–2235. <https://doi.org/10.1002/ijc.25861>

Bakiri, L., and E.F. Wagner. 2013. Mouse models for liver cancer. *Mol. Oncol.* 7: 206–223. <https://doi.org/10.1016/j.molonc.2013.01.005>

Bosch, F.X., J. Ribes, M. Díaz, and R. Cléries. 2004. Primary liver cancer: worldwide incidence and trends. *Gastroenterology*. 127(5, Suppl 1): S5–S16. <https://doi.org/10.1053/j.gastro.2004.09.011>

Böttner, A., J. Kratzsch, G. Müller, T.M. Kapellen, S. Blüher, E. Keller, M. Blüher, and W. Kiess. 2004. Gender differences of adiponectin levels develop during the progression of puberty and are related to serum androgen levels. *J. Clin. Endocrinol. Metab.* 89:4053–4061. <https://doi.org/10.1210/jc.2004-0303>

Bray, F., J. Ferlay, I. Soerjomataram, R.L. Siegel, L.A. Torre, and A. Jemal. 2018. Global cancer statistics 2018: GLOBOCAN estimates of incidence and mortality worldwide for 36 cancers in 185 countries. *CA Cancer J. Clin.* 68:394–424. <https://doi.org/10.3322/caac.21492>

Chen, H.P., J.J. Shieh, C.C. Chang, T.T. Chen, J.T. Lin, M.S. Wu, J.H. Lin, and C. Y. Wu. 2013. Metformin decreases hepatocellular carcinoma risk in a

dose-dependent manner: population-based and in vitro studies. *Gut*. 62: 606–615. <https://doi.org/10.1136/gutjnl-2011-301708>

Cheung, O.K., and A.S. Cheng. 2016. Gender Differences in Adipocyte Metabolism and Liver Cancer Progression. *Front. Genet.* 7:168. <https://doi.org/10.3389/fgene.2016.00168>

Combs, T.P., A.H. Berg, M.W. Rajala, S. Klebanov, P. Iyengar, J.C. Jimenez-Chillaron, M.E. Patti, S.L. Klein, R.S. Weinstein, and P.E. Scherer. 2003. Sexual differentiation, pregnancy, calorie restriction, and aging affect the adipocyte-specific secretory protein adiponectin. *Diabetes*. 52: 268–276. <https://doi.org/10.2337/diabetes.52.2.268>

Dalamaga, M., K.N. Diakopoulos, and C.S. Mantzoros. 2012. The role of adiponectin in cancer: a review of current evidence. *Endocr. Rev.* 33: 547–594. <https://doi.org/10.1210/er.2011-1015>

Fuente-Martín, E., P. Argente-Arizón, P. Ros, J. Argente, and J.A. Chowen. 2013. Sex differences in adipose tissue: It is not only a question of quantity and distribution. *Adipocyte*. 2:128–134. <https://doi.org/10.4161/adip.24075>

Ghebranos, N., and S. Sell. 1998. Hepatitis B injury, male gender, aflatoxin, and p53 expression each contribute to hepatocarcinogenesis in transgenic mice. *Hepatology*. 27:383–391. <https://doi.org/10.1002/hep.510270211>

Goodman, Z.D. 2007. Grading and staging systems for inflammation and fibrosis in chronic liver diseases. *J. Hepatol.* 47:598–607. <https://doi.org/10.1016/j.jhep.2007.07.006>

Havel, P.J. 2002. Control of energy homeostasis and insulin action by adipocyte hormones: leptin, acylation stimulating protein, and adiponectin. *Curr. Opin. Lipidol.* 13:51–59. <https://doi.org/10.1097/00041433-200202000-00008>

Heindryckx, F., I. Colle, and H. Van Vlierberghe. 2009. Experimental mouse models for hepatocellular carcinoma research. *Int. J. Exp. Pathol.* 90: 367–386. <https://doi.org/10.1111/j.1365-2613.2009.00656.x>

Hui, L., L. Bakiri, A. Mairhorfer, N. Schweifer, C. Haslinger, L. Kenner, V. Kommenovic, H. Scheuch, H. Beug, and E.F. Wagner. 2007. p38alpha suppresses normal and cancer cell proliferation by antagonizing the JNK-c-Jun pathway. *Nat. Genet.* 39:741–749. <https://doi.org/10.1038/ng2033>

Kotani, K., K. Wakai, A. Shibata, Y. Fujita, I. Ogimoto, M. Naito, Y. Kurozawa, H. Suzuki, T. Yoshimura, A. Tamakoshi, and J.S. Group. JACC Study Group. 2009. Serum adiponectin multimer complexes and liver cancer risk in a large cohort study in Japan. *Asian Pac. J. Cancer Prev.* 10(suppl): 87–90.

Larsson, S.C., and A. Wolk. 2007. Overweight, obesity and risk of liver cancer: a meta-analysis of cohort studies. *Br. J. Cancer*. 97:1005–1008. <https://doi.org/10.1038/sj.bjc.6603932>

Luo, Z., M. Zang, and W. Guo. 2010. AMPK as a metabolic tumor suppressor: control of metabolism and cell growth. *Future Oncol.* 6:457–470. <https://doi.org/10.2217/fon.09.174>

Ma, S.J., Y.X. Zheng, P.C. Zhou, Y.N. Xiao, and H.Z. Tan. 2016. Metformin use improves survival of diabetic liver cancer patients: systematic review and meta-analysis. *Oncotarget*. 7:66202–66211.

Manieri, E., and G. Sabio. 2015. Stress kinases in the modulation of metabolism and energy balance. *J. Mol. Endocrinol.* 55:R11–R22. <https://doi.org/10.1530/JME-15-0146>

Mao, X., J.Y. Hong, and L.Q. Dong. 2006a. The adiponectin signaling pathway as a novel pharmacological target. *Mini Rev. Med. Chem.* 6:1331–1340. <https://doi.org/10.2174/138955706778992978>

Mao, X., C.K. Kikani, R.A. Riojas, P. Langlais, L. Wang, F.J. Ramos, Q. Fang, C. Y. Christ-Roberts, J.Y. Hong, R.Y. Kim, et al. 2006b. APPL1 binds to adiponectin receptors and mediates adiponectin signalling and function. *Nat. Cell Biol.* 8:516–523. <https://doi.org/10.1038/ncb1404>

Marquardt, J.U., J.B. Andersen, and S.S. Thorgeirsson. 2015. Functional and genetic deconstruction of the cellular origin in liver cancer. *Nat. Rev. Cancer*. 15:653–667. <https://doi.org/10.1038/nrc4017>

Naugler, W.E., T. Sakurai, S. Kim, S. Maeda, K. Kim, A.M. Elsharkawy, and M. Karin. 2007. Gender disparity in liver cancer due to sex differences in MyD88-dependent IL-6 production. *Science*. 317:121–124. <https://doi.org/10.1126/science.1140485>

Nishizawa, H., I. Shimomura, K. Kishida, N. Maeda, H. Kuriyama, H. Nagaretani, M. Matsuda, H. Kondo, N. Furuyama, S. Kihara, et al. 2002. Androgens decrease plasma adiponectin, an insulin-sensitizing adipocyte-derived protein. *Diabetes*. 51:2734–2741.

Parkin, D.M., F. Bray, J. Ferlay, and P. Pisani. 2005. Global cancer statistics, 2002. *CA Cancer J. Clin.* 55:74–108. <https://doi.org/10.3322/canjclin.55.2.74>

- Polyzos, S.A., J. Kountouras, C. Zavos, and E. Tsiaousi. 2010. The role of adiponectin in the pathogenesis and treatment of non-alcoholic fatty liver disease. *Diabetes Obes. Metab.* 12:365–383. <https://doi.org/10.1111/j.1463-1326.2009.01176.x>
- Sabio, G., M. Das, A. Mora, Z. Zhang, J.Y. Jun, H.J. Ko, T. Barrett, J.K. Kim, and R.J. Davis. 2008. A stress signaling pathway in adipose tissue regulates hepatic insulin resistance. *Science*. 322:1539–1543. <https://doi.org/10.1126/science.1160794>
- Salguero Palacios, R., M. Roderfeld, S. Hemmann, T. Rath, S. Atanasova, A. Tschuschner, O.A. Gressner, R. Weiskirchen, J. Graf, and E. Roeb. 2008. Activation of hepatic stellate cells is associated with cytokine expression in thioacetamide-induced hepatic fibrosis in mice. *Lab. Invest.* 88: 1192–1203. <https://doi.org/10.1038/labinvest.2008.91>
- Sharma, D., J. Wang, P.P. Fu, S. Sharma, A. Nagalingam, J. Mells, J. Handy, A.J. Page, C. Cohen, F.A. Anania, and N.K. Saxena. 2010. Adiponectin antagonizes the oncogenic actions of leptin in hepatocellular carcinogenesis. *Hepatology*. 52:1713–1722. <https://doi.org/10.1002/hep.23892>
- Wang, Z.V., and P.E. Scherer. 2016. Adiponectin, the past two decades. *J. Mol. Cell Biol.* 8:93–100. <https://doi.org/10.1093/jmcb/mjw011>
- Whitehead, J.P., A.A. Richards, I.J. Hickman, G.A. Macdonald, and J.B. Prins. 2006. Adiponectin—a key adipokine in the metabolic syndrome. *Diabetes Obes. Metab.* 8:264–280. <https://doi.org/10.1111/j.1463-1326.2005.00510.x>
- Yamauchi, T., J. Kamon, Y. Minokoshi, Y. Ito, H. Waki, S. Uchida, S. Yamashita, M. Noda, S. Kita, K. Ueki, et al. 2002. Adiponectin stimulates glucose utilization and fatty-acid oxidation by activating AMP-activated protein kinase. *Nat. Med.* 8:1288–1295. <https://doi.org/10.1038/nm788>
- Yannakoulia, M., N. Yiannakouris, S. Blüher, A.L. Matalas, D. Klimis-Zacas, and C.S. Mantzoros. 2003. Body fat mass and macronutrient intake in relation to circulating soluble leptin receptor, free leptin index, adiponectin, and resistin concentrations in healthy humans. *J. Clin. Endocrinol. Metab.* 88:1730–1736. <https://doi.org/10.1210/jc.2002-021604>

Supplemental material

Manieri et al., <https://doi.org/10.1084/jem.20181288>

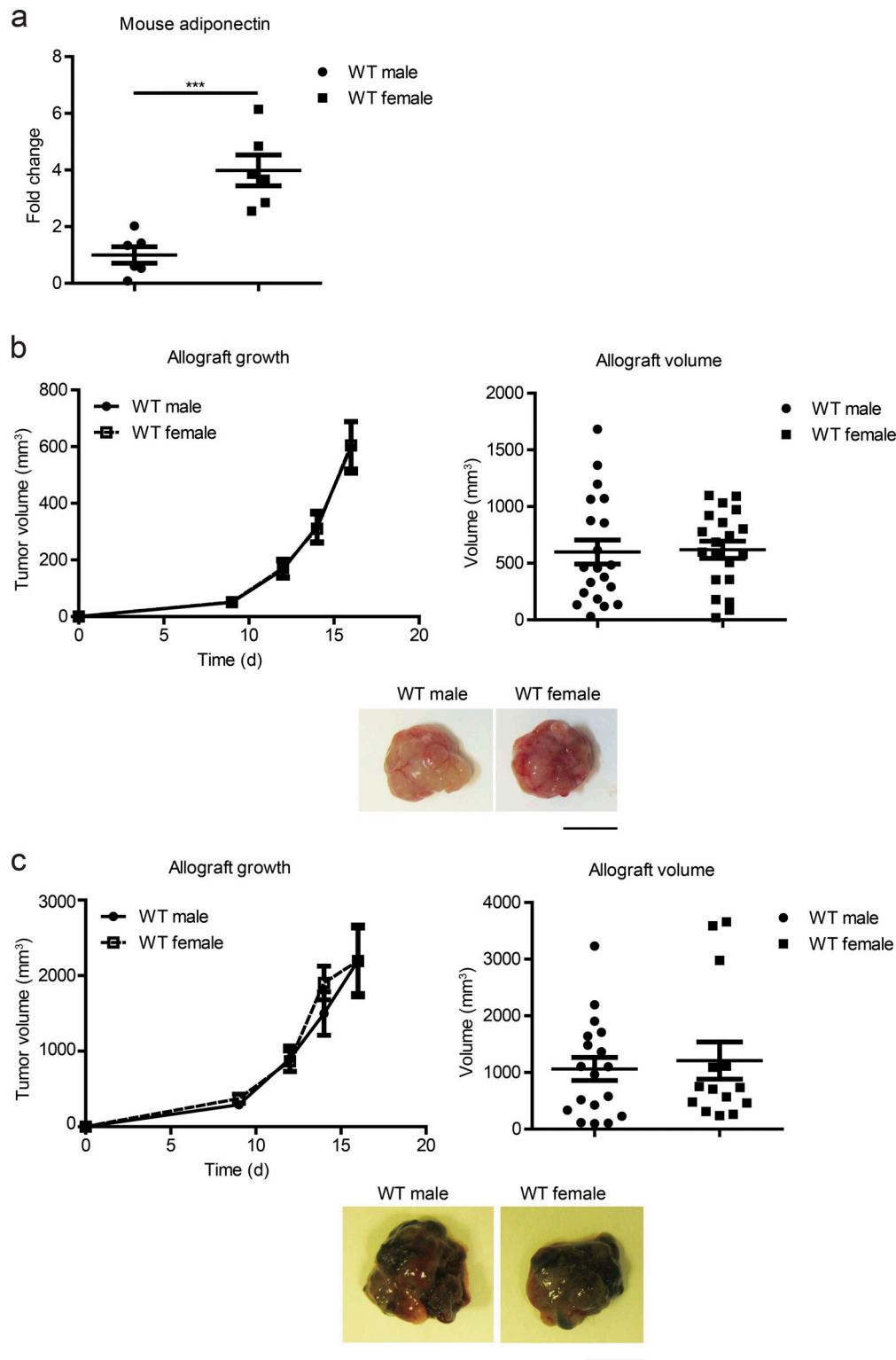


Figure S1. **Adiponectin quantification and specificity of gender differences in HCC.** (a) Circulating levels of adiponectin were measured in 11–12-wk-old female and male mice. Data are normalized to male mice and shown as means \pm SEM; ***, $P < 0.001$; Student's t test; $n = 6$. (b) Representative allografts and tumor volume quantification in WT male and female mice during the experiment and at sacrifice 3 wk after subcutaneous injection with 5×10^5 MC-38 cells (colon adenocarcinoma-derived cells) in each flank. Data are shown as means \pm SEM; nonsignificant differences were found; two-way ANOVA coupled with Bonferroni's multiple comparisons test (allograft growth); Student's t test (allograft volume); $n = 20$ tumors (10 mice per genotype). Bar, 1 cm. (c) Representative allografts and tumor volume quantification in WT male and female mice during the experiment and at sacrifice 2 wk after subcutaneous injection with 5×10^5 B16-F10 cells (melanoma-derived cells) in each flank. Data are shown as means \pm SEM; nonsignificant differences were found; two-way ANOVA coupled with Bonferroni's multiple comparisons test (allograft growth); Student's t test (allograft volume); WT male $n = 18$ tumors (10 mice); WT female $n = 14$ tumors (7 mice). Bar, 1 cm.

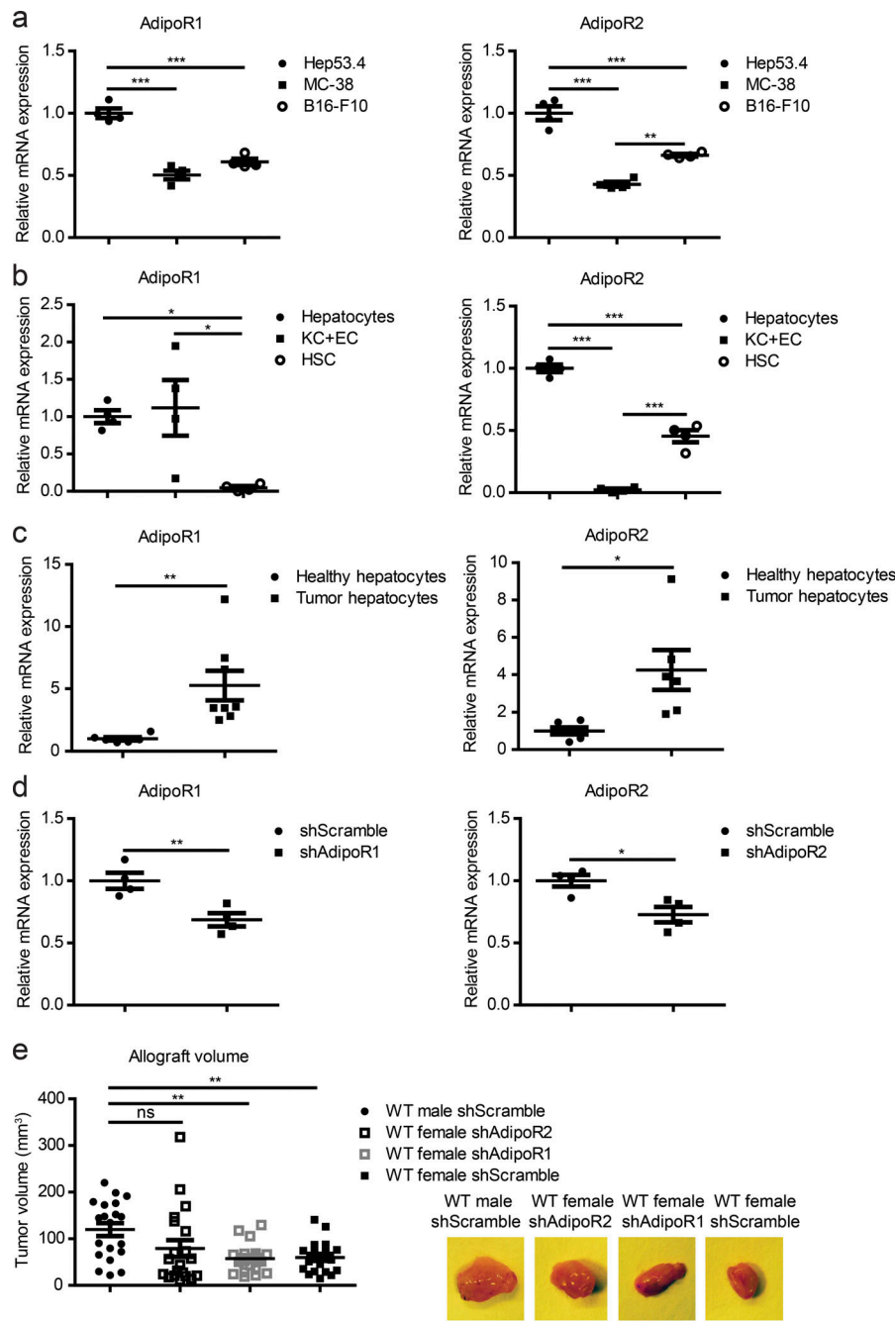


Figure S2. Analysis of adiponectin receptors expression and their role in tumor growth. (a) qRT-PCR analysis of adiponectin receptors 1 and 2 (*AdipoR1* and *AdipoR2*) in Hep53.4, MC-38, or B16-F10 tumor cells. mRNA expression was normalized to the amount of *Gapdh* mRNA in each sample. Data are normalized to Hep53.4 cells and shown as means \pm SEM; **, $P < 0.01$; ***, $P < 0.001$; one-way ANOVA coupled with Bonferroni's multiple comparisons test; $n = 4$. **(b)** qRT-PCR analysis of *AdipoR1* and *AdipoR2* in different liver cell populations. mRNA expression was normalized to the amount of *Gapdh* mRNA in each sample. Data are normalized to hepatocytes and shown as means \pm SEM; *, $P < 0.05$; ***, $P < 0.001$; one-way ANOVA coupled with Bonferroni's multiple comparisons test; $n = 4$. **(c)** qRT-PCR analysis of *AdipoR1* and *AdipoR2* in healthy hepatocytes and hepatocytes derived from hepatic tumors of C57BL/6J mice treated with DEN at P14 and 300 μ g/liter TAA administered in the drinking water for 26 wk. mRNA expression was normalized to the amount of *Gapdh* mRNA in each sample. Data are normalized to healthy hepatocytes and shown as means \pm SEM; *, $P < 0.05$; **, $P < 0.01$; Student's *t* test with Welch's correction; healthy hepatocytes $n = 6$; tumor hepatocytes $n = 6-8$. **(d)** qRT-PCR analysis of *AdipoR1* in Hep53.4 treated with a shRNA against *AdipoR1* (shAdipoR1) or a scrambled control sequence, and analysis of *AdipoR2* in Hep53.4 cells treated with a shRNA against *AdipoR2* (shAdipoR2) or a scrambled control sequence. mRNA expression was normalized to the amount of *Gapdh* mRNA in each sample. Data are normalized to shScramble cells and shown as means \pm SEM; *, $P < 0.05$; **, $P < 0.01$; Student's *t* test; $n = 4$. **(e)** Representative allografts and tumor volume quantification in WT mice with hepatic tumors lacking *AdipoR1* or *AdipoR2* expression. Mice received subcutaneous injections with 1×10^6 Hep53.4 cells per flank, previously transduced with shRNA targeting *AdipoR1*, *AdipoR2* or a control sequence (shScramble). Mice were sacrificed 3 wk after Hep53.4 cell injection. Data are shown as means \pm SEM; **, $P < 0.01$; nonsignificant differences (ns); one-way ANOVA coupled with Bonferroni's multiple comparisons test; WT $n = 20$ tumors (10 mice per group), except WT female shAdipoR1 $n = 18$ tumors (10 mice). Bar, 1 cm.

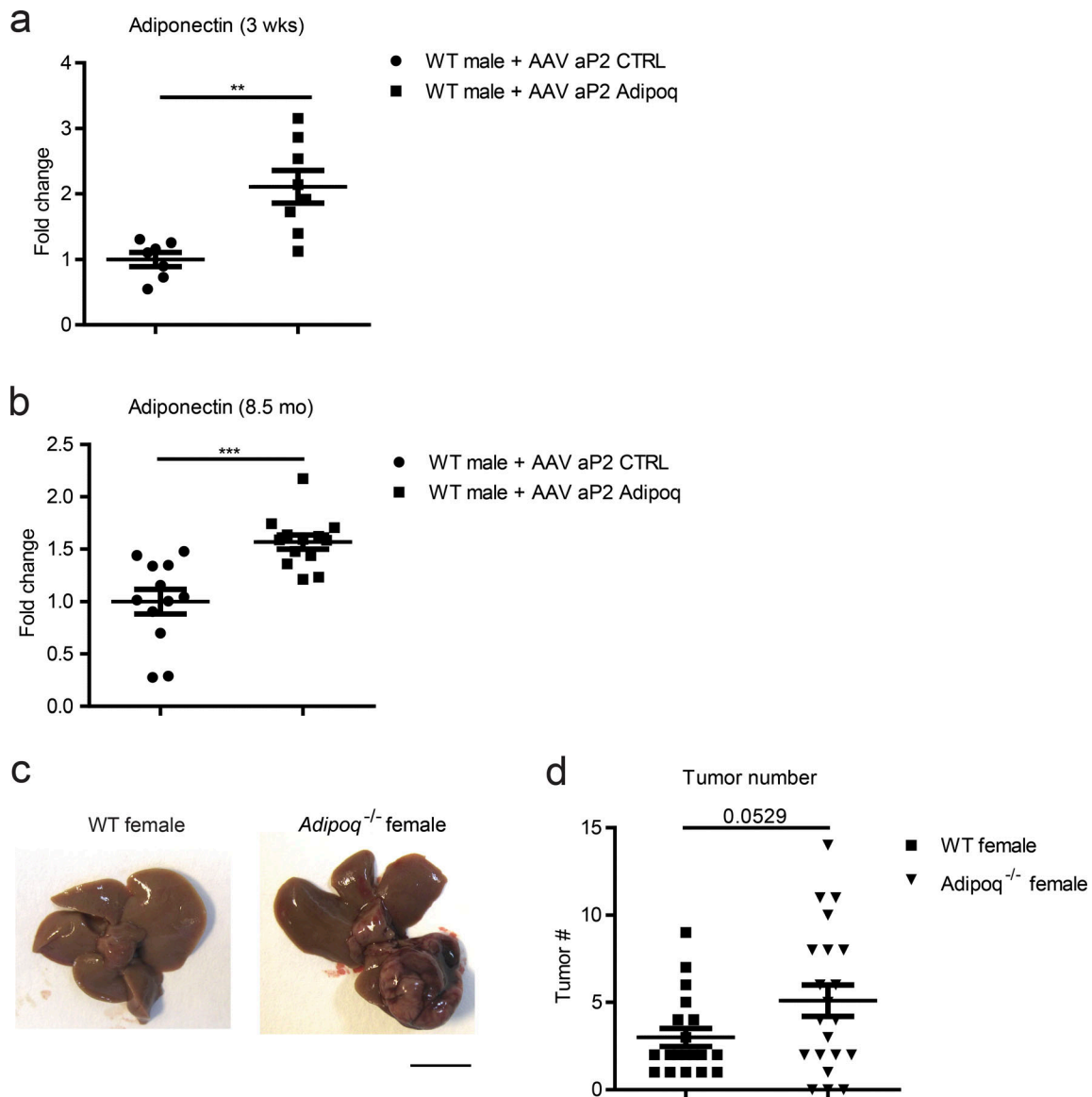


Figure S3. **Adiponectin quantification and overexpression in mice and effect of adiponectin deficiency in female mice.** **(a and b)** 6–7-wk-old WT male mice were injected with adeno-associated virus carrying a control sequence (WT male + AAV aP2 CTRL) or the adiponectin gene under control of the aP2 promoter (WT male + AAV aP2 Adipoq) at P1 and received an i.p. DEN injection (50 mg/kg body weight) 14 d later. AAV, adeno-associated virus; CTRL, control. **(a)** Quantification of circulating levels of adiponectin 3 wk after virus injection. Data are shown as means \pm SEM; **, $P < 0.01$; Student's *t* test with Welch's correction; WT male + AAV aP2 CTRL $n = 7$; WT male + AAV aP2 Adipoq $n = 8$. **(b)** Quantification of circulating levels of adiponectin 8.5 mo after virus injection. Data are shown as means \pm SEM; ***, $P < 0.001$; Student's *t* test; WT male + AAV aP2 CTRL $n = 12$; WT male + AAV aP2 Adipoq $n = 13$. **(c)** HCC development 8 mo after i.p. injection with DEN (50 mg/kg) on P14 in WT and *Adipoq*^{-/-} female mice. Bar, 1 cm. **(d)** Tumor number was determined at sacrifice. Data are shown as means \pm SEM; Student's *t* test with Welch's correction; WT female $n = 19$; *Adipoq*^{-/-} female $n = 21$.

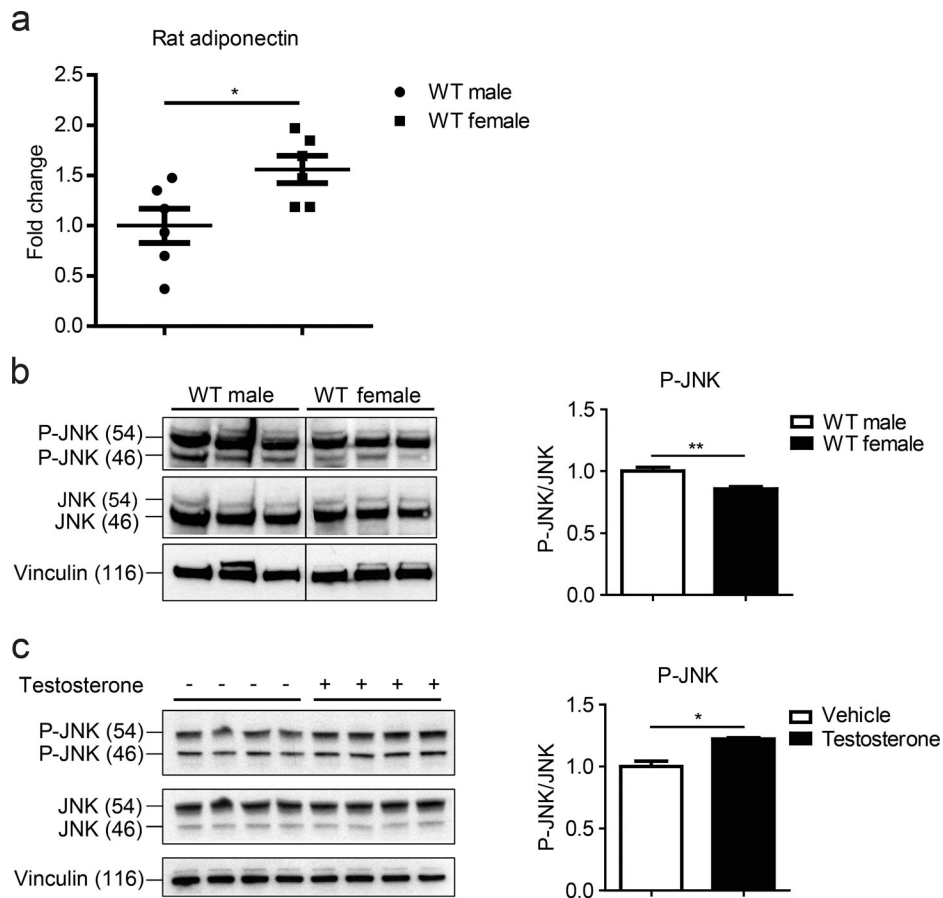


Figure S4. **Gender disparity in rat adiponectin, mice adipose tissue, and human adipocytes JNK phosphorylation.** (a) Circulating levels of adiponectin were measured in WT male and female rats. Data are normalized to male rats. Data are shown as means \pm SEM; *, $P < 0.05$; Student's t test; $n = 6$. (b) Immunoblot analysis and quantification of phospho-JNK and JNK in adipose tissue from WT male and female mice. Vinculin protein expression was monitored as a loading control. Data are shown as means \pm SEM; **, $P < 0.01$; Student's t test; WT male $n = 3$; WT female $n = 4$. (c) Immunoblot analysis and quantification of phospho-JNK and JNK in human differentiated adipocytes after treatment with testosterone (1,200 nM for 30 min). Vinculin protein expression was monitored as a loading control. Data are shown as means \pm SEM; *, $P < 0.05$; Student's t test with Welch's correction; $n = 4$.

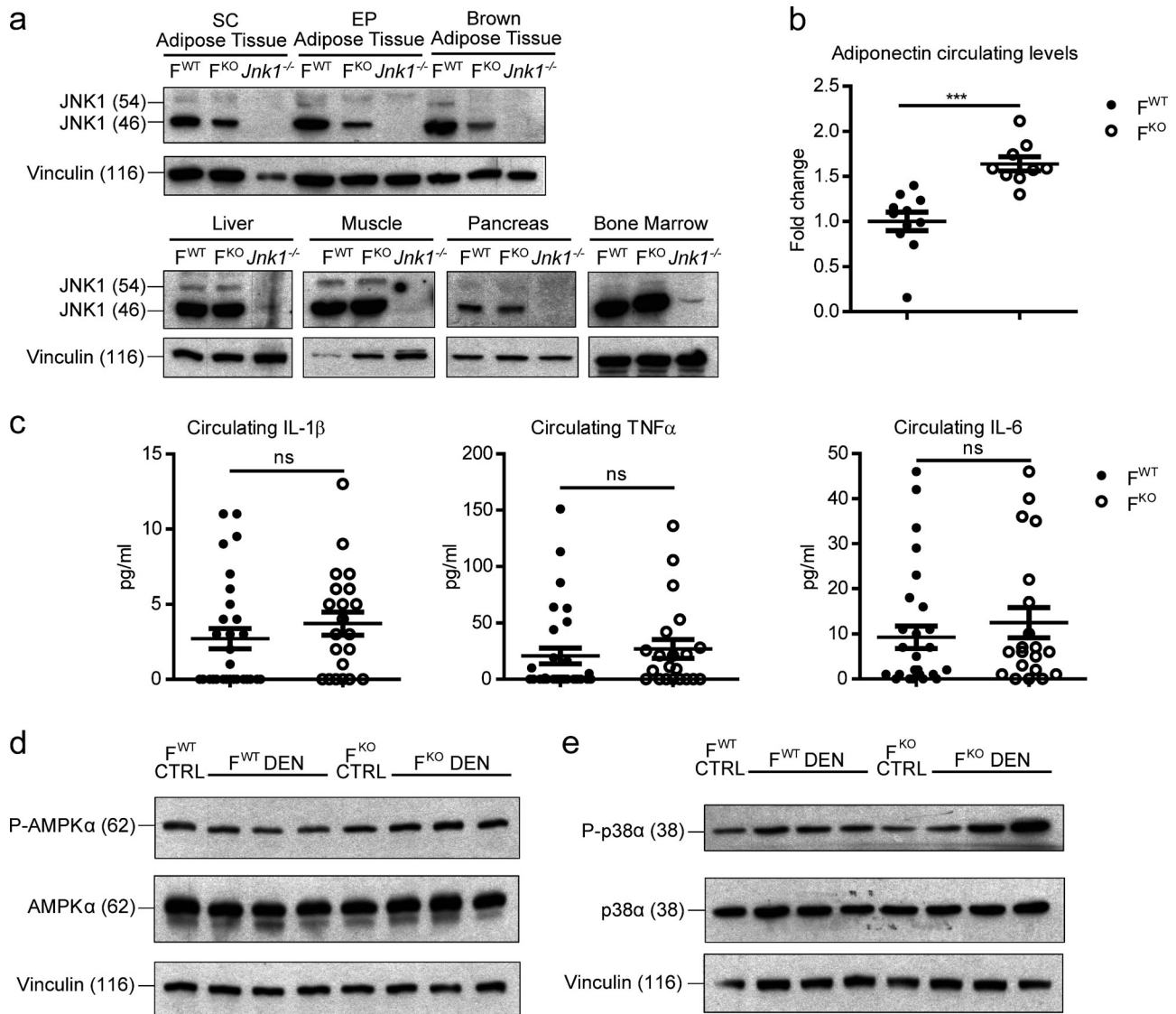


Figure S5. **Deletion of JNK1, cytokines levels in *F^{WT}* and *F^{KO}* mice, and adiponectin protection through AMPK α and p38 α activation.** (a) Control (*F^{WT}*) and adipose tissue JNK1-deficient (*F^{KO}*) mice were sacrificed at 10 wk, and different tissues were extracted and analyzed by immunoblotting. Tissues from *Jnk1^{-/-}* mice were used as a control. EP, epididymal; SC, subcutaneous. Vinculin protein expression was monitored as a loading control. (b) Circulating levels of adiponectin were measured in control (*F^{WT}*) and adipose tissue JNK1-deficient (*F^{KO}*) mice. Data are normalized to *F^{WT}* adiponectin levels and are shown as means \pm SEM; ***, $P < 0.001$; Student's *t* test; *F^{WT}* $n = 11$; *F^{KO}* $n = 9$. (c) Control (*F^{WT}*) and adipose tissue JNK1-deficient (*F^{KO}*) mice were injected i.p. with DEN (50 mg/kg) on P14. Serum was analyzed after 8 mo on a Luminex platform to measure the levels of TNF α , IL-1 β , and IL-6 adipokines. Data are shown as means \pm SEM; nonsignificant differences were found (ns); Student's *t* test; $n = 20$ –30. (d and e) *F^{WT}* and *F^{KO}* mice were injected i.p. with DEN (50 mg/kg) or saline (CTRL) on P14. (d) Immunoblot analysis of phospho-AMPK α , AMPK α , and vinculin in livers obtained 1 mo after DEN injection. (e) Immunoblot analysis of phospho-p38 α , p38 α , and vinculin in livers obtained 1 mo after DEN injection.

Table S1. **Characteristics of women and men**

| Variable | Women (n = 9) | Men (n = 10) | P value |
|---------------------------------|----------------------|---------------------|----------------|
| Age (yr) | 49.7 (14.3) | 58.1 (14.3) | 0.278 |
| Hypertension (n) | 1 (11.1) | 2 (20) | 0.542 |
| Diabetes mellitus (n) | 0 | 0 | - |
| BMI (kg/m ²) | 25.8 (3.5) | 26.8 (4.5) | 0.905 |
| Fasting blood sugar (mg/dl) | 86.1 (12.8) | 99 (10.5) | 0.046 |
| AST (IU/liter) | 24.3 (12.9) | 21.1 (5.1) | 0.798 |
| ALT (IU/liter) | 32.5 (32.2) | 30.3 (20.7) | 0.878 |
| Alkaline phosphatase (IU/liter) | 77.4 (21.4) | 95.3 (35.3) | 0.536 |
| Bilirubin (mg/dl) | 0.5 (0.3) | 0.9 (0.5) | 0.059 |
| Albumin (mg/dl) | 4.5 (0.3) | 4.5 (0.6) | 0.607 |
| Total cholesterol (mg/dl) | 205.9 (50) | 189.9 (47.9) | 0.383 |
| Triglycerides (mg/dl) | 118.7 (67.5) | 116 (49.7) | 0.902 |
| LDL-cholesterol (mg/dl) | 121.7 (44.5) | 123.7 (43.7) | 0.945 |
| HDL-cholesterol (mg/dl) | 62.1 (14.6) | 42.9 (12.7) | 0.035 |
| Adiponectin (μg/ml) | 19.69 (2.663) | 14.18 (3.620) | 0.0016 |

Variables are presented as mean (SD) or absolute frequency (%) and are compared by means of Mann-Whitney *U* test or χ^2 test. ALT, alanine aminotransferase; AST, aspartate aminotransferase; BMI, body mass index; HDL, high-density lipoprotein; LDL, low-density lipoprotein.

Table S2. **qRT-PCR primers**

| Gene | Forward primer (5'→3') | Reverse primer (5'→3') |
|----------------|-------------------------------|-------------------------------|
| <i>AdipoR1</i> | AATGGGGCTCCTTCTGGTAAC | GGATGACTCTCCAACGTCCCT |
| <i>AdipoR2</i> | GGCCCATCATGCTATGGAAC | GTGAGGGATCACTCGCCATC |
| <i>Gapdh</i> | TGAAGCAGGCATCTGAGGG | CGAAGGTGGAAGAGTGGGA |

Table S3. **Solutions for hepatic perfusion**

| Solution (ml) | A | B | C | D |
|--------------------------|----------|----------|----------|----------------|
| SC-1 | 100 | - | - | - |
| SC-2 | - | 100 | 100 | 100 |
| DNase I (stock solution) | - | - | - | 1 ^a |
| Collagenase D (mg) | - | - | 110 | 80 |
| Pronase E (mg) | - | 40 | - | 50 |

^aDNase I stock solution: 2 mg/ml in GBSS-B.

Table S4. **Stock solutions for hepatic cell isolation**

| Stock solution (mg) | SC1 | SC2 | GBSS-A | GBSS-B |
|---|------------|------------|---------------|---------------|
| EGTA | 95 | - | - | - |
| Glucose | 450 | - | 495.5 | 495.5 |
| HEPES | 1,190 | 1,190 | - | - |
| KCl | 200 | 200 | 185 | 185 |
| Na ₂ HPO ₄ ·2H ₂ O | 75.5 | 75.5 | 37.5 | 37.5 |
| NaCl | 4,000 | 4,000 | - | 4,000 |
| NaH ₂ PO ₄ ·H ₂ O | 39 | 39 | - | - |
| NaHCO ₃ | 175 | 175 | 113.5 | 113.5 |
| Phenol Red | 3 | 3 | 3 | 3 |
| CaCl ₂ ·2H ₂ O | - | 280 | 112.5 | 112.5 |
| KH ₂ PO ₄ | - | - | 15 | 15 |
| MgCl ₂ ·6H ₂ O | - | - | 105 | 105 |
| MgSO ₄ ·7H ₂ O | - | - | 35 | 35 |
| H ₂ O to (ml) | 500 | 500 | 500 | 500 |

For the density gradient medium, the following solutions were prepared before starting the perfusion of the liver: Nycodenz 1: 5.18 g/total volume 15 ml GBSS-A; Nycodenz 2: 3.63 g/total volume 25 ml GBSS-A.